



HAL
open science

Scintillating fibre based beta spectrometer: Proof of concept by Monte-Carlo simulation and first experimental assessment

Nicolas Dufour, Adrien Sari, Guillaume H. V. Bertrand, Frédéric Carrel

► To cite this version:

Nicolas Dufour, Adrien Sari, Guillaume H. V. Bertrand, Frédéric Carrel. Scintillating fibre based beta spectrometer: Proof of concept by Monte-Carlo simulation and first experimental assessment. Nuclear Instruments and Methods in Physics Research Section A: Accelerators, Spectrometers, Detectors and Associated Equipment, 2021, 1010, 165548 (7 p.). 10.1016/j.nima.2021.165548 . cea-04550635

HAL Id: cea-04550635

<https://cea.hal.science/cea-04550635>

Submitted on 17 Apr 2024

HAL is a multi-disciplinary open access archive for the deposit and dissemination of scientific research documents, whether they are published or not. The documents may come from teaching and research institutions in France or abroad, or from public or private research centers.

L'archive ouverte pluridisciplinaire **HAL**, est destinée au dépôt et à la diffusion de documents scientifiques de niveau recherche, publiés ou non, émanant des établissements d'enseignement et de recherche français ou étrangers, des laboratoires publics ou privés.

Scintillating fibre based beta spectrometer: proof of concept by Monte-Carlo simulation and first experimental assessment

N. Dufour^{*1}, A. Sari¹, G. H. V. Bertrand¹, F. Carrel¹

¹Université Paris-Saclay, CEA, List, F-91120 Palaiseau, France

^{*}nicolas.dufour3@cea.fr

Abstract

We developed a new beta measurement method based on scintillating fibres, able to discriminate incident beta particles based on their energy, using various cladding thicknesses, which could find useful applications in the field of nuclear decommissioning and dismantling (D&D). Indeed, thanks to Monte Carlo simulations, we found that high-energy beta particles were less affected by thicker cladding than medium-energy beta particles. Therefore, combining different cladding thicknesses and a deconvolution method, we were able to identify and quantify convoluted beta spectra in a simulated scenario. In this paper, we describe the Monte Carlo simulations combined with the deconvolution algorithm based on the Maximum Likelihood – Expectation Maximization method (ML-EM), and the associated experimental setup. We demonstrated the feasibility of such a method, using both simulated and experimental data, by deconvoluting ³⁶Cl and ⁹⁰Sr–⁹⁰Y spectra, considering ³⁶Cl as a medium-energy beta emitter and ⁹⁰Sr–⁹⁰Y as a high-energy beta emitter. Using fibres with only one thickness of cladding, we found that we could not estimate both contributions correctly, with errors reaching up to 71% of the actual activities. However, using two different acquisitions of fibres each one with a different cladding thickness, we were able to estimate both contributions with an error of 26% for ³⁶Cl and 10% for ⁹⁰Sr–⁹⁰Y. Study of the improvement of these performances is presented and could help to fine-tune activities estimated. The next step of this work would consist in designing a beta spectrometer, based on scintillating fibres, and assess its performances. Taking advantage of both deformability capacity of scintillating fibres and their potential lengths up to a few meters, we expect that such a detection system will be well adapted to the radiological characterization of large surfaces, and suitable for deployment on uneven surfaces.

I. Introduction

Once a nuclear facility has ceased its activity, nuclear decommissioning and dismantling (D&D) ensures that all contamination is removed and treated accordingly. Depending on the past operations conducted in the facility, expected contamination hotspots can vary in terms of radionuclides present and associated activities. Different particles can be emitted by a single radioactive spot, thus hampering the characterization of a particular signal. For example, ⁹⁰Sr is a fission product, beta emitter only, found along with ¹³⁷Cs, beta and gamma emitter. On-site characterization of ⁹⁰Sr contamination can be estimated using scaling factors between ⁹⁰Sr and ¹³⁷Cs [1], but this methodology can only be applied where such scaling factors exist, such as in nuclear power plants [2] only under the hypothesis that these scaling factors are applicable and correct. Moreover, this method cannot be applied in cases in which the beta contamination is not linked with a gamma emitter. Different detectors and methodology have been developed specifically to resolve this problem [3]–[6]. Since the emission spectrum of a beta particle is continuous, there are no characteristic figures to rely on in order to identify beta emitters. Thus, deterministic and statistical analysis were developed in order to deconvolute beta spectra [7]–[9]. A new technical solution based on the usage of plastic scintillating fibres (PSF) with various cladding thicknesses, and a deconvolution method using Maximum Likelihood-Expectation Maximisation (ML-EM) [10], is presented in this paper. This new technical solution is adapted to the radiological characterization of large surfaces, and able to fit uneven surfaces from the intrinsic deformability of scintillating fibres.

PSF used in this study are composed of a core made in polystyrene, and a cladding primarily made in polymethylmethacrylate (PMMA). Both materials are composed of elements characterized by low atomic numbers, carbon and hydrogen. Thus, an organic scintillating fibre is intrinsically less sensitive to gamma-rays than beta particles, reducing any parasite signal coming from gamma emitters. PSF can be manufactured with lengths up to a few meters, first from a polymerisation step and then a fiber-drawing step. Such methodology is described in more details in the literature [11]. Applications of PSF are various and range from particle tracking [12], the detection of radionuclides in drinking water [13], to high-energy calorimetry [14]. Using their deformability capabilities, PSF would enable the detector to adapt to the measured surface, reducing losses due to the air layer when measuring beta particles, and enabling a better radiological characterization of uneven surfaces.

In this paper, we study the feasibility of a beta spectrometer based on scintillating fibres. First, we will present the principle of the separation of two convoluted beta signals based on Monte Carlo simulation, combined with the ML-EM algorithm. Then, we will present the experimental setup and the results, obtained using ³⁶Cl and ⁹⁰Sr–⁹⁰Y beta sources, used to evaluate the methodology of using scintillating fibres with various cladding thicknesses, combined

61 with the ML-EM algorithm. This methodology showed an improvement of the deconvolution process, especially in the
62 determination of the high-energy beta emitter.

63

64 II. Monte Carlo simulation and radionuclide identification

65

66 A. Principle and simulation study

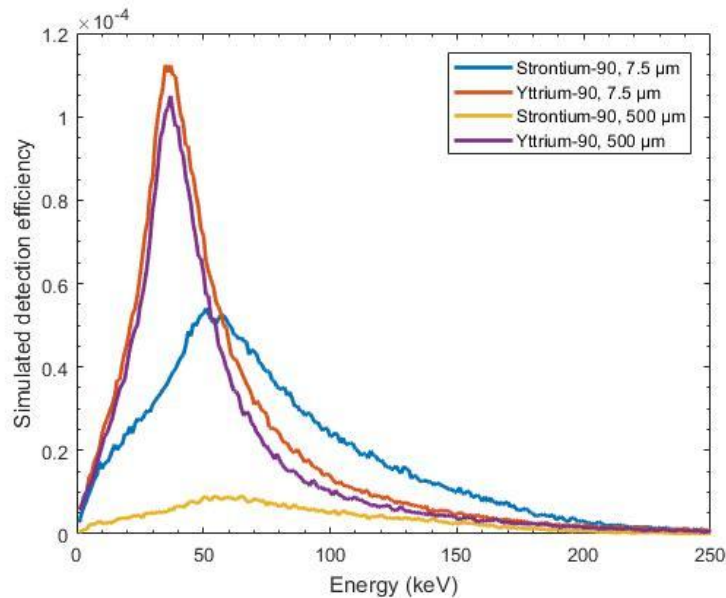
67

68 In the research and development of nuclear detectors, a simulation phase is classic as it allows an estimation of the
69 detector response, amongst other calculations, before any experimental measurements. As such, using the MCNP6.2
70 simulation code [15], we designed the geometry of a single polystyrene scintillating fibre and studied its response
71 when exposed to beta sources. The simulated fibre consists of a polystyrene core with a diameter of 250 μm , and two
72 cladding thicknesses were simulated: 7.5 μm and 500 μm , both in PMMA. Sources used were pure-beta emitters ^{90}Sr
73 and ^{90}Y , generated using the BetaShape software [16]. The mentioned radionuclides were chosen for their disparities
74 in their beta emission spectrum: ^{90}Sr has a beta energy endpoint at 546 keV and an average beta energy of 196 keV,
75 while these values are 2280 keV and 926 keV respectively for ^{90}Y . We calculated the deposited energy spectra from
76 incident beta particles normalised per emitted particle, called the F8 tally in MCNP6.2. Without further considerations,
77 we can estimate that the F8 tally result is comparable to a detection efficiency; therefore, we will designate the result
78 as a simulated detection power of polystyrene. Results of the simulations are presented in figure 1, and figure 2 presents the
79 electronic stopping power of polystyrene.

80

81

82



83

84

85

Fig. 1. Simulated detection efficiency as a function of beta particle energy, simulated with MCNP6.2 for different beta radionuclides. One standard deviation uncertainties are shown.

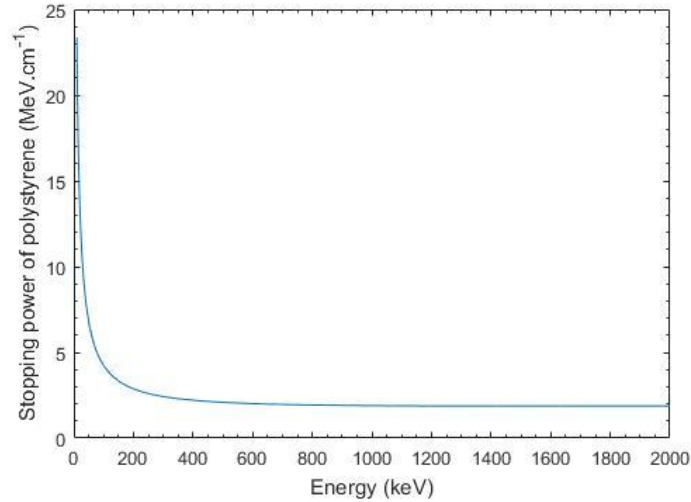


Fig. 2. Electronic stopping power of polystyrene ($\rho = 1.05$). Data collected from ESTAR [17].

86
87
88 These results illustrate the impact of the cladding. More specifically, ^{90}Y data show the same peak centered around
89 40 keV, for both cladding thicknesses. A partial energy deposit, characterized by a constant energy deposition rate of
90 the high-energy beta particles can explain this peak. Indeed, the stopping power of polystyrene for electrons between
91 500 keV and 2 MeV is equal to 2 MeV/cm, as shown in figure 2. Calculation of the deposited energy in 250 μm of
92 polystyrene crossed gives 50 keV, which is coherent with our simulation and shows that these particles do not deposit
93 all of their energy. Higher energy depositions are explained by electron paths greater than 250 μm , expected for any
94 non-perpendicular incident vector or any diffusion inside the fibre. The limited impact of the cladding to the peak is
95 explained by a low energy deposition in the PMMA. Indeed, energy deposition in 7.5 μm and 500 μm of PMMA is
96 1 keV and 75 keV respectively, when the electron energy is comprised between 500 keV and 2 MeV. Thus, any
97 electron with an incident energy greater than 575 keV will induce the same stopping power in polystyrene whether
98 there is a 500 μm cladding or not. Therefore, high-energy beta emitters will yield the same peak whether the cladding
99 is 7.5 μm or 500 μm .

100 However, the decrease for the ^{90}Sr signal is significant, and is due to the energy deposition in the cladding being
101 more important. From figure 2, we can see that the polystyrene stopping power increases exponentially as the electron
102 energy decreases below 500 keV, this phenomenon being also found for PMMA. Since ^{90}Sr beta emission spectrum
103 ranges from 0 to 546 keV, we expect all electrons emitted to be affected by the thicker cladding. For example, the
104 average ^{90}Sr beta particle of 196 keV will deposit 2 keV for 7.5 μm of PMMA, but will not go through 500 μm of
105 PMMA. The energy deposition for a cladding of 500 μm will change the electronic stopping power from 2.7 MeV/cm
106 to 3.6 MeV/cm. Therefore, any expected spectrum at 7.5 μm cladding will be different from a 500 μm cladding
107 spectrum, combined with a shielding effect blocking low-energy beta particles.

108 We conclude that a contrast was achieved, with a low impact on the high-energy beta emitter, and a significant
109 decrease of the medium-energy beta emitter. Therefore, by using scintillating fibres with various cladding thicknesses,
110 we expect to be able to create a contrast between different beta distributions. By using more scintillating fibres with
111 different cladding thicknesses, we expect contrasts to be sufficient to identify and quantify beta signatures. However,
112 such a detection system would require the use of a deconvolution algorithm to interpret the measurements. In the
113 frame of this study, we chose the Maximum Likelihood – Expectation Maximisation (ML-EM).

114

115 B. Identification with ML-EM

116

117 The Maximum Likelihood – Expectation Maximisation (ML-EM) algorithm is a method used in matrix inversion
118 problems. It is based on an iterative calculation of the maximum likelihood achievable between an input dataset and a
119 predetermined database, where the input dataset follows a Poisson distribution. The iterative nature of the ML-EM
120 approach ensures the convergence of the calculated estimation, but imposes the definition of a starting value and a
121 next sequence step equation. Mathematical development leading to the final equation for the ML-EM resolution has
122 already been detailed in the literature [10], [18], [19], and more specifically to gamma-ray spectra deconvolution [20]–
123 [22]. A general formula for the number of measured counts from a radioactive source can be written as:

124

$$Y = A_{source} I \varepsilon t \quad (1)$$

125

126 With Y the measured spectrum, A_{source} the source activity, I the emission intensity of the measured particle, ε the
 127 detection efficiency and t the measurement time. The equation can be simplified using λ as the total number of
 128 emitted particles by the source, over the measurement time t , factored by the emission intensity I :
 129

$$\lambda = A_{source} I t \quad (2)$$

130
 131 Considering each bin of the measured spectrum, Y can be seen as a vector of B values (for *Binning*), each value
 132 describing one energy bin. In such case, there is a specific detection efficiency for each bin corresponding to the
 133 particle energy, thus ε has at least one dimension. Moreover, if there are multiple sources tested, λ can be seen as a
 134 matrix of S values (for *Sources*). Therefore, ε must possess another dimension corresponding to the detection
 135 efficiency for each radionuclide. For example, if we have a sampling of 1024 values for each spectrum, the dimension
 136 of Y will be [1024,1]. Moreover, if we evaluate the contribution of three possible beta emitters, dimension of ε will be
 137 [1024, 3], representing the three detection efficiency spectra for each beta source. Then, the dimension of λ will be
 138 [1,3].

139 We can rewrite equation 1 using matrix notations

$$[Y]_B = [\lambda]_S [\varepsilon]_{B,S} \quad (3)$$

141
 142 The measured spectrum matrix $[Y]_B$ is obtained through measurements, $[\varepsilon]_{B,S}$ is the associated database of detection
 143 efficiencies and $[\lambda]_S$ is the emission spectrum, which is the desired information from the deconvolution process. The
 144 detection efficiency database $[\varepsilon]_{B,S}$ is an array composed of each detection efficiency corresponding to each
 145 radioactive source evaluated. This database can be generated through Monte Carlo simulations or experimental data.

146 Let $\hat{\lambda}$ be the estimator of λ . The ML-EM expression for the methodology defines the following next sequence step
 147 equation:

148

$$\hat{\lambda}_j^{(n+1)} = \frac{\hat{\lambda}_j^{(n)}}{\sum_{i=1}^B \varepsilon_{i,j}} \sum_{i=1}^B \frac{\varepsilon_{i,j} Y_i}{\sum_{k=1}^S \varepsilon_{i,k} \hat{\lambda}_k^{(n)}} \quad (4)$$

149 Where $\hat{\lambda}_j^{(n+1)}$ is the estimator for the emission spectrum. Since the ML-EM algorithm is iterative, $\hat{\lambda}_j^{(n+1)}$ is the
 150 estimator at the $n + 1$ step, $\hat{\lambda}_j^{(n)}$ is the estimator at the n step, i represents the iterator linked to the binning dimension
 151 and both j and k are iterators linked to the source dimension. The first value, at the $n = 1$ step, must be input.
 152 Following [23], the first value can be the average value written as:

153

$$\hat{\lambda}_j^{(1)} = \frac{\sum_{i=1}^B Y_i}{\sum_{i=1}^B \sum_{j=1}^S \varepsilon_{i,j}} \quad (5)$$

154
 155 We simulated the response of the scintillating fibre with other beta emission spectra: ^{14}C , ^{90}Sr , ^{90}Y , ^{210}Bi , ^{212}Bi and
 156 ^{212}Pb , for the two cladding thicknesses previously mentioned: 7.5 μm and 500 μm , in the same fashion as the results
 157 presented in figure 1. To do so, we used MCNP6.2 to calculate the simulated detection efficiencies for each source,
 158 using the F8 tally. This dataset was then used to construct a database of responses, corresponding to the $\varepsilon_{i,j}$ matrix, by
 159 merging all F8 tally results. The input spectrum Y_i consisted of the simulation of a measured spectrum of ^{90}Sr and ^{90}Y ,
 160 in secular equilibrium, with a total activity of 2000 Bq. To construct this simulated measured spectrum, we added both
 161 ^{90}Sr and ^{90}Y simulated detection efficiencies, and multiplied the result with the simulated activity of 2000 Bq.
 162 Furthermore, to simulate the uncertainty associated with the counting statistics, each bin of the simulated measured
 163 spectrum was varied using a Poisson law. We expect a perfect identification and quantification for an ML-EM
 164 reconstructed activity of ^{90}Sr and ^{90}Y equal to 1000 Bq, and other radionuclides to 0 Bq. Table 1 presents the ML-EM
 165 results, for 200 iterations. The number of iterations was chosen based on the convergence of the ML-EM output
 166 values.

167

168

	^{14}C	^{90}Sr	^{90}Y	^{210}Bi	^{212}Bi	^{212}Pb
Input activity (Bq)	0	1000	1000	0	0	0
Reconstructed	<1	963	990	5	<1	19

activity (Bq)						
---------------	--	--	--	--	--	--

169 Table 1. Input and reconstructed activities using the ML-EM algorithm.
170

171 From these results, we validated the methodology of using scintillating fibres with various cladding thicknesses to
172 create a discrimination between beta emission spectra. This enables the use of deconvolution methods allowing to
173 identify and quantify beta emitters present in an unknown mixture. We note that the ML-EM algorithm has a threshold
174 below which identification may not be certain, as it can be seen on the reconstructed activity of ^{212}Pb . From the
175 validation of the concept using simulations, we developed a setup to assess the experimental feasibility of the
176 methodology.

177

178 III. Experimental setup and acquisitions

179

180 A. Methods and materials

181

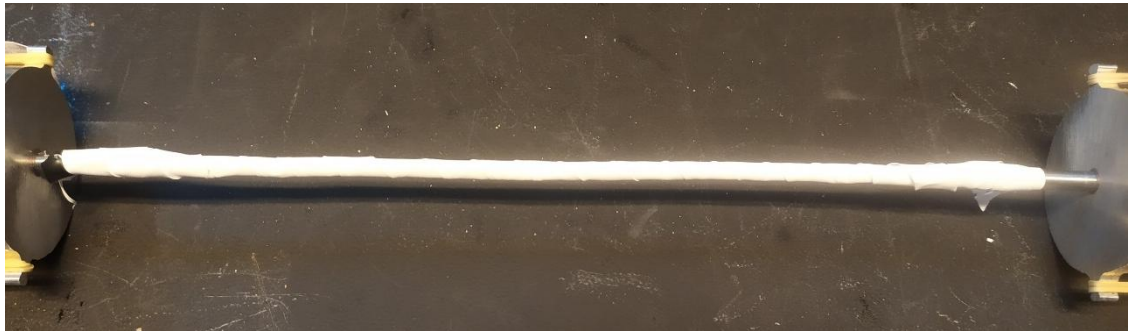
182 Following simulation results, we developed an experimental setup to evaluate the feasibility of the methodology
183 presented above. A PSF bundle was manufactured and is composed of one hundred BCF-10 scintillating fibres [24]
184 mounted onto two photomultiplier tubes 9205SB [25] using homemade adaptors. We chose one hundred scintillating
185 fibres instead of a single one, similar to the simulation results presented above, because a single fibre was not enough
186 to obtain a measurable signal. Optical grease has been applied to the interface. A single fibre has a core diameter of
187 250 μm and a surrounding optical cladding of 7.5 μm -thick. Fibre core is made of polystyrene and cladding is made of
188 polymethyl methacrylate (PMMA). Voltage applied to the photomultiplier tubes (PMTs) was 850 V. Anode outputs
189 are linked to a CAEN DT5743 digitizer [26], and measurements were done in coincidence to reduce background
190 signal. The coincidence windows was taken with a value of 15 ns, corresponding to the temporal length of a pulse.
191 Experimental setup has been placed in a dark environment, inside a metallic box, preventing any visible light to
192 interfere. A photography of the experimental setup inside the box is shown in figure 3. Cladding thickness was
193 modified using layers of PTFE. Each layer of PTFE is 200 μm -thick. Up to four were used one on the top of each
194 other to obtain a total thickness of 800 μm as is shown in figure 4. One acquisition set was done without any layer.
195

196



196 Fig. 3. Photography of the experimental setup with scintillating fibres. The bundle of fibres is shown in the middle. The
197 aluminium adaptors to the PMTs are also visible, the mechanical pressure between the fibres and PMTs being exerted by the rubber
198 bands. In the middle is the source holder. Both black cylinders, on the left and right hand sides, are the PMTs.
199

200



201 Fig. 4. Photography of the experimental setup with scintillating fibres and four PTFE layers stacked (total thickness of 800 μm).
202

203

204 Table 2 sums the characteristics of the two beta sources we used, ^{36}Cl and ^{90}Sr - ^{90}Y . They were chosen for the
205 difference in energy distribution and endpoint. Data listed in table 2 was taken from the Nucléide LARA database
206 [27].

207

	Chlorine-36	Strontium-90 + Yttrium-90
Activity	$6470 \pm 320 \text{ Bq}$	$5170 \pm 260 \text{ Bq}$

Particles emitted	Beta ¹	Beta
Average beta energy (keV)	246.5 keV	195.9 keV (⁹⁰ Sr) 933 keV (⁹⁰ Y)
Maximum beta energy (keV)	709.3 keV	546.2 keV (⁹⁰ Sr) 2281.5 keV (⁹⁰ Y)

208 Table 2. List of radioactive beta sources used during our measurement campaign. Uncertainties given at one standard deviation.

209 ¹We will consider ³⁶Cl as a pure beta emitter since the other decay line possible is of low intensity (β^+ , 1.9%).

210

211 *B. Acquisition results – Single source measurement*

212

213 The first set of measurements was done with a single source during each acquisition. Figure 5 presents
 214 experimental data for the naked fibre bundle and 800 μm of PTFE, and figure 6 presents the summed detection
 215 efficiency of each spectrum, as a function of the PTFE thickness. For visualisation purposes, the detection
 216 efficiency scale is constant for both graphs in figure 5. Horizontal axis in figure 5 is shown in pC units, and
 217 corresponds to the charge of the digitized pulse. This is a standard output of the CAEN DT5743 digitizer and allows
 218 the construction of an acquisition histogram.

219

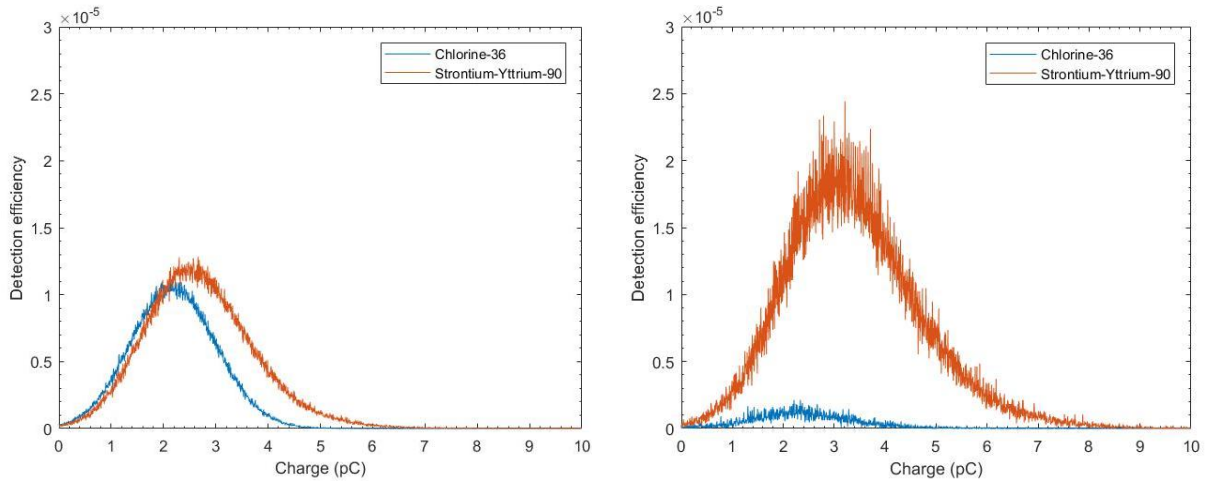


Fig. 5. Detection efficiency of the fibre bundle without any PTFE layer on the left, and with 800 μm of PTFE on the right, for the ^{36}Cl and ^{90}Sr - ^{90}Y sources.

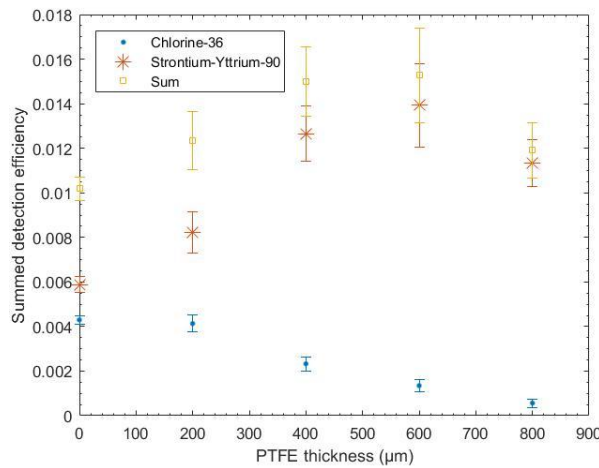


Fig. 6. Summed detection efficiency as a function of the PTFE thickness, for the ^{36}Cl and ^{90}Sr - ^{90}Y sources. One standard deviation uncertainties are shown.

220
221
222
223

224
225
226
227

Detection efficiency for the ^{36}Cl source tends towards zero as more and more layers of PTFE are added, with a slower decrease from 0 μm to 200 μm compared with the thicker layers, visible in figure 6. ^{90}Sr - ^{90}Y detection efficiency does not follow the same trend. Indeed, detection efficiency increases until 600 μm , before decreasing. In parallel to this phenomenon, we also note that the maximum pulse charge has also slightly increased. In figure 5 for the naked bundle, ^{90}Sr - ^{90}Y detection efficiency curve reaches zero at 7 pC, while it reaches 0 at 9 pC for 800 μm of PTFE. We explain both of these effects from the increase of the trapping efficiency. Indeed, a naked BCF-10 fibre has a trapping efficiency of 3.44% [13], meaning that 96.56% of all generated scintillation photons are lost. Adding a reflecting layer of PTFE increases the percentage of captured photons. A better trapping efficiency allows more photons to be detected, increasing both the detection efficiency and the maximum resulting charge. However, energy loss due to thicker layers of PTFE will overlap the benefits of a better trapping efficiency, as can be seen for the detection efficiency for ^{90}Sr - ^{90}Y , decreasing after 600 μm of PTFE.

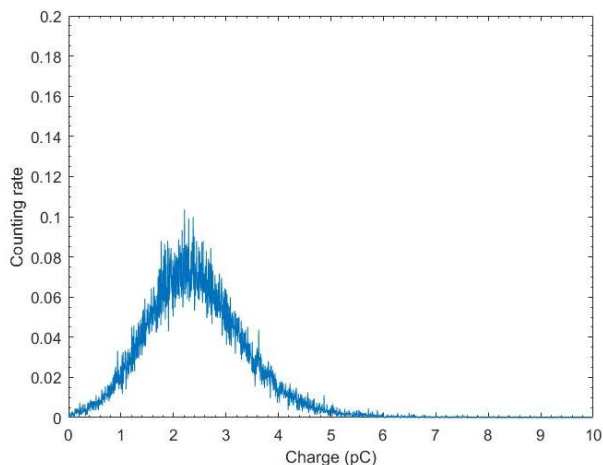
Overall, for the ^{90}Sr - ^{90}Y source, we can hypothesize that only the most energetic part of the emission spectrum is detected, thus the impact from the strontium part of the beta emission spectrum is negligible. Even though the trapping efficiency is maximised when adding PTFE, this increase does not compensate for the energy loss of ^{36}Cl beta particles crossing the cladding, for all thicknesses. Therefore, from these first experimental results, we demonstrate the feasibility of the multi-cladding PSF detector principle, to develop a beta counter able to discriminate incident beta particles in gross energy ranges.

245

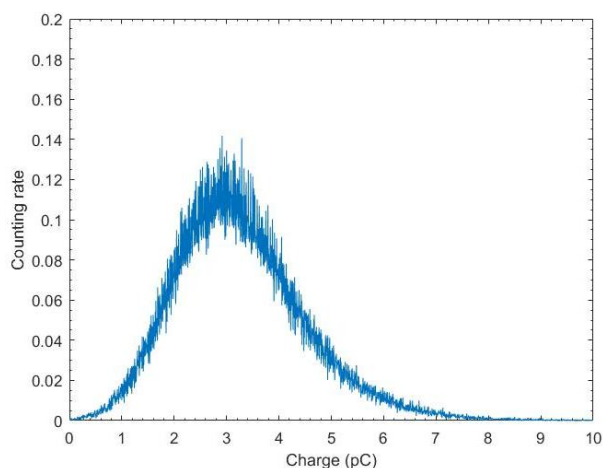
246 *C. Acquisition results – Double source measurement*

247

248 In this section, we will evaluate the detector's response when two beta source are placed together, to check if we
 249 find any discrepancies with single source acquisitions. Moreover, this data will be used as the input data for testing
 250 ML-EM algorithm performances. In this set of measurements, the two beta sources used, ^{36}Cl and ^{90}Sr - ^{90}Y , were
 251 measured simultaneously for the different thicknesses of PTFE. Figure 7 present the measurements results for both
 252 the naked bundle and with 800 μm of PTFE, expressed in counting rate (s^{-1}). For visualisation purposes, the
 253 counting rate scale is constant for figure 7. Figure 8 shows the summed counting rate for each thickness of PTFE.
 254

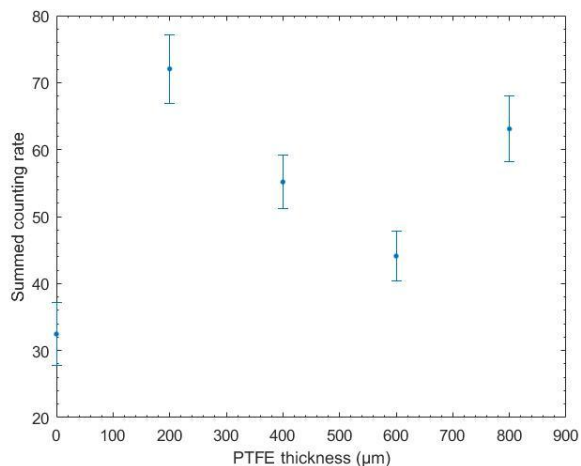


255



256
 257
 258
 259

Fig. 7. Fibre bundle counting rate when both sources are present, with no PTFE layer on the left and with 800 μm of PTFE on the right.



260
 261
 262

Fig. 8. Summed counting rate as a function of the PTFE thickness applied to the bundle, for dual sources measurements. One standard deviation uncertainties are shown.

263

264 The distribution endpoint can help identifying the most energetic beta emitter radionuclide, from the maximum
265 charge read, but not identify precisely any other beta emitter. However, even in a lack of prior information point-of-
266 view, we would be able to say that the measured sample contains at least one high-energy beta emitter, since an
267 800 μm-thick PTFE layer was not able to stop incident radiations, under the hypothesis that the signal is in fact due
268 to beta particles.

269 When both sources are present, behaviours described for the single source measurements are not visible here.
270 Indeed, figure 6 shows a constant increase of the summed detection efficiency up to 600 μm and a slight decrease at
271 800 μm for the sum, while the behaviour in figure 8 is not similar. Thus, there is a discrepancy between summed
272 mono-sources measurements and dual sources measurements. Causes for this discrepancy may be due to
273 differences in geometrical efficiency, and an inhomogeneity of the PTFE layers, discussed in more detail in the
274 spectrum identification section of this article.

275 From the highest contrast achieved with the thickest layer of PTFE, we expect the ML-EM code to correctly
276 evaluate high-energy beta emitters, and then deduce medium-energy beta emitters present on the other acquisition
277 spectra. As we have seen, single source acquisitions show some limitations concerning the representativity of single
278 source measurements. To tackle this issue, we are studying possible improvements of the experimental setup,
279 especially concerning the homogeneity of PTFE layers, and ensuring that they do not overlap or loosen. In order to
280 obtain better results, new protocols with three or more sources are being studied and should provide information
281 about limitations on the identification and quantification processes, in terms of number of sources present.

282

283 IV. Spectrum identification

284

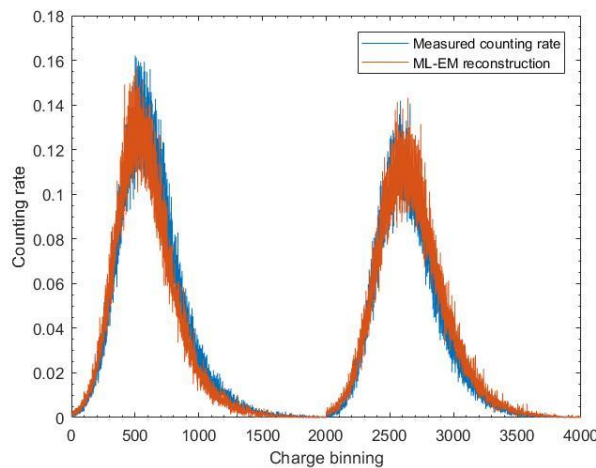
285 A. Deconvolution results – Dual sources measurements with various cladding thicknesses

286

287 Using single source acquisitions as the ML-EM database, we tested the algorithm ability to separate the ³⁶Cl and
288 ⁹⁰Sr-⁹⁰Y beta spectra, from the double source acquisitions. We chose two thicknesses for the database, 200 μm and
289 800 μm of PTFE, because of the high contrast between ³⁶Cl and ⁹⁰Sr-⁹⁰Y detection efficiency spectra (*cf.* figs. 4 and 5).
290 Moreover, we empirically found better ML-EM reconstructions using these two spectra, and a comparatively worse
291 reconstruction using any other combinations, including all acquisition spectra together. This behaviour will be
292 discussed in the next section. One hundred iterations were enough for the convergence of ML-EM output data, and are
293 presented in figure 9.

294

295



296

297 Fig. 9. Measured spectra and ML-EM reconstruction of the counting rate, for 200 μm of PTFE on the left and 800 μm on the
298 right, when both ³⁶Cl and ⁹⁰Sr-⁹⁰Y sources are present.

299

300 No visual discrepancies are visible between experimental data and the ML-EM reconstruction. Actual sources
301 activities and the ML-EM reconstructed counterpart are presented in table 3. Percentage biases were calculated in
302 order to evaluate the difference between experimental and ML-EM reconstructed activities.

303

	Source activity	Reconstructed activity	Percentage biases
--	-----------------	------------------------	-------------------

Chlorine-36	6470 ± 324 Bq	4780 Bq	-26%
Strontium-Yttrium-90	5168 ± 258 Bq	5776 Bq	+12%

Table 3. Sources and ML-EM reconstructed activities for 200 μ m and 800 μ m spectra inputs.

Comparing data from table 3, we can see that the ^{36}Cl reconstructed activity does not match the experimental value, with an underestimation over five standard deviations. However, ^{90}Sr - ^{90}Y activity is correct under three standard deviations. Discrepancies will be discussed by comparing obtained results with expected ones.

B. Deconvolution results – Dual sources measurements with a single cladding thickness

In order to validate the methodology, we tested the ML-EM reconstruction using only one acquisition spectrum. Table 4 presents the ML-EM reconstructed activities using single spectrum databases, and their associated percentage biases. Each ML-EM column corresponds to a database and measured spectrum couple, corresponding to measurements done using the specified PTFE layer. For example, ML-EM – 0 μ m corresponds to the construction of a database using single source measurements with no layers of PTFE, and the measured spectrum corresponds to the measurement of both sources together without PTFE.

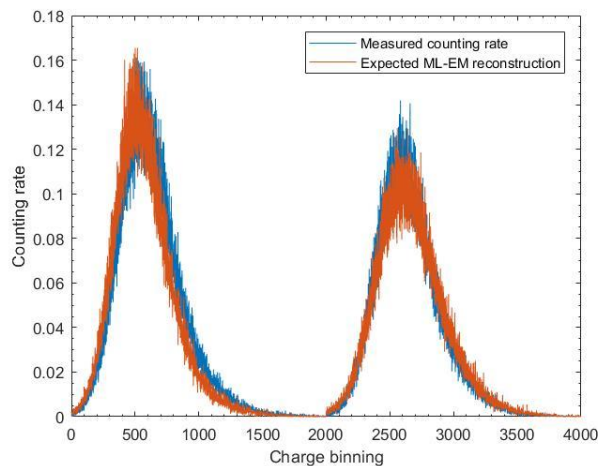
	^{36}Cl	^{36}Cl percentage bias	^{90}Sr - ^{90}Y	^{90}Sr - ^{90}Y percentage bias
Source activity	6470 ± 324 Bq	N/A	5168 ± 258 Bq	N/A
ML-EM – 0 μ m	4136 Bq	-36%	2552 Bq	-51%
ML-EM – 200 μ m	1852 Bq	-71%	7844 Bq	+52%
ML-EM – 400 μ m	9313 Bq	+44%	2678 Bq	-48%
ML-EM – 600 μ m	6962 Bq	+8%	2502 Bq	-52%
ML-EM – 800 μ m	9348 Bq	+44%	5103 Bq	-1%

Table 4. Sources and ML-EM reconstructed activities, with associated percentage biases, for single spectrum databases.

Comparing table 4 with table 3 percentage biases, we note that some single PTFE thickness configurations obtain better results on a single beta emitter than with two PTFE thicknesses configurations. For example, 800 μ m PTFE single spectrum obtains a percentage bias of 1% with the expected ^{90}Sr - ^{90}Y activity, but has a percentage bias of 44% with the expected ^{36}Cl activity. On the other hand, 600 μ m PTFE single spectrum obtains a percentage bias of 8% with the expected ^{36}Cl activity, but has a percentage bias of 52% with the expected ^{90}Sr - ^{90}Y activity. From the percentage bias values in table 3, 26% and 12% for the ^{36}Cl and ^{90}Sr - ^{90}Y respectively, we conclude that the methodology presented here constitutes the best compromise for the deconvolution of the two beta spectra.

C. Deconvolution results – Expected results

Considering the database, we calculated the expected spectra if the reconstructed activities were correct, *i.e.* equal to the experimental activities presented in table 3, for the setup with 200 and 800 μ m of PTFE. Figure 10 presents the expected reconstructed spectrum.



336 Fig. 10. Measured spectra and expected ML-EM reconstruction of the counting rate for exact activities, for 200 μm of PTFE on
337 the left and 800 μm on the right, when both ^{36}Cl and ^{90}Sr - ^{90}Y sources are present.

338
339 Both figs. 11 and 12 are similar in shape and intensity without any major visual discrepancy. We do note that the
340 expected ML-EM reconstruction of figure 10 does not overlap completely the measured counting rate on the second
341 peak, while it is the case for figure 9. Average maximum value for both measured and reconstructed spectra for the
342 second peak in figure 9 is 0.13 s^{-1} , while for figure 10, average maximum value is 0.11 s^{-1} for the expected ML-EM
343 reconstruction: even when using the experimental activities, we obtain a slight difference between the experimental
344 spectra and reconstructed ones. We explain this difference from a lack of representativeness of the database, possibly
345 due to statistical variation at the maximum peak values. Another factor may be the solid angle differences being too
346 important between one source and two sources measurements. However, we do not expect significant differences,
347 because sources were placed together along the fibres bundle, only shifting their position from the single source
348 location by a few centimetres. In addition, we note that PTFE layers were changed or readjusted between
349 measurements for the database and dual sources acquisitions. PTFE thicknesses may not have been consistent and thus
350 created discrepancies. From this study, we conclude that the small variations may impede the correct reconstruction.

351

352 Conclusion and outlook

353

354 We recall that the objective of this paper was to develop a new methodology of beta identification and
355 quantification system using scintillating fibres, to tackle the issue of radiological characterization of large and possible
356 uneven surfaces. In this paper, we presented the principle of a discrimination method based on scintillating fibres with
357 various cladding thicknesses, for medium and high-energy beta emitters, enabling beta spectrometry using
358 deconvolution algorithms. We studied using Monte Carlo simulation the methodology principle by identifying and
359 quantifying beta signatures using the ML-EM algorithm. A database of multiple simulated beta signatures was
360 constructed and used effectively with satisfying deconvolution results. Then, an experimental setup was designed, and
361 showed that the methodology can be used on a detection system. First results showed an improvement of the
362 identification and quantification of convoluted beta emitters when compared to single cladding scintillating fibers
363 presented in IV. B.

364 Further, we plan to acquire spectra with longer measurement time to construct a database with less statistical
365 variation and check the prevalence of this issue on the representativity. Moreover, we are planning to manufacture
366 specific bundles with preset PTFE layers. These improvements will help in developing a first prototype of beta
367 spectrometer using Monte Carlo simulation and then assess its performances in laboratory. Two application layouts
368 are studied: spectrometry using deconvolution algorithms like presented in this paper, and a counting mode, where
369 identification is limited to the energy range of the beta emitter, for example, between medium and high-energy beta
370 emitter. In this case, there would be no need for a deconvolution methodology. Studies with more than two beta
371 sources present are planned, and will cover larger energy ranges. Studies of the actual detector sensitivity to gamma
372 rays is currently underway. Finally, study of the counting rate evolution as a function of the detector deformability is
373 also planned.

374

375

- 377
- 378 [1] W. Irrek, K. Müller, D. Fouquet, and A. P. Froggatt, "Comparison among different decommissioning funds
379 methodologies for nuclear installations," 2007.
- 380 [2] *Radiological Characterization of Shut Down Nuclear Reactors for Decommissioning Purposes*, no. 389.
381 Vienna: International Atomic Energy Agency, 1998.
- 382 [3] A. R. Lang *et al.*, "Cesium and Strontium Contamination of Nuclear Plant Stainless Steel: Implications for
383 Decommissioning and Waste Minimization," *ACS Omega*, vol. 4, no. 11, pp. 14420–14429, Sep. 2019.
- 384 [4] G. Turkington, K. A. A. Gamage, and J. Graham, "Beta detection of strontium-90 and the potential for
385 direct in situ beta detection for nuclear decommissioning applications," *Nucl. Instruments Methods Phys.
386 Res. Sect. A Accel. Spectrometers, Detect. Assoc. Equip.*, vol. 911, pp. 55–65, Dec. 2018.
- 387 [5] A. Leskinen, P. Fichet, M. Siitari-Kauppi, and F. Goutelard, "Digital autoradiography (DA) in
388 quantification of trace level beta emitters on concrete," *J. Radioanal. Nucl. Chem.*, vol. 298, no. 1, pp. 153–
389 161, Oct. 2013.
- 390 [6] P. Fichet, A. Leskinen, S. Guegan, and F. Goutelard, "Characterization of Beta Emitters for
391 Decommissioning," in *Volume 2: Facility Decontamination and Decommissioning; Environmental
392 Remediation; Environmental Management/Public Involvement/Crosscutting Issues/Global Partnering*,
393 2013.
- 394 [7] A. Grau Malonda, L. Rodriguez Barquero, and A. Grau Carles, "Radioactivity determination of ^{90}Y , ^{90}Sr
395 and ^{89}Sr mixtures by spectral deconvolution," *Nucl. Instruments Methods Phys. Res. Sect. A Accel.
396 Spectrometers, Detect. Assoc. Equip.*, vol. 339, no. 1–2, pp. 31–37, Jan. 1994.
- 397 [8] T. M. Semkow, "Statistical deconvolution of beta spectra: Implications for neutrino mass detection," *Appl.
398 Radiat. Isot.*, vol. 46, no. 5, pp. 341–349, May 1995.
- 399 [9] R. Remetti and A. Sessa, "Beta spectra deconvolution for liquid scintillation counting," *J. Radioanal. Nucl.
400 Chem.*, vol. 287, no. 1, pp. 107–111, Jan. 2011.
- 401 [10] L. A. Shepp and Y. Vardi, "Maximum Likelihood Reconstruction for Emission Tomography," *IEEE Trans.
402 Med. Imaging*, vol. 1, no. 2, pp. 113–122, Oct. 1982.
- 403 [11] P. Rebourgeard *et al.*, "Fabrication and measurements of plastic scintillating fibers," *Nucl. Instruments
404 Methods Phys. Res. Sect. A Accel. Spectrometers, Detect. Assoc. Equip.*, vol. 427, no. 3, pp. 543–567, May
405 1999.
- 406 [12] R. E. Ansorge *et al.*, "The UA2 scintillating fibre detector," *Nucl. Inst. Methods Phys. Res. A*, vol. 273, no.
407 2–3, pp. 826–832, 1988.
- 408 [13] T. Bernard *et al.*, "SAFEWATER – Innovative Tools for the Detection and Mitigation of CBRN Related
409 Contamination Events of Drinking Water," *Procedia Eng.*, vol. 119, pp. 352–359, 2015.
- 410 [14] H. Burmeister, "Electromagnetic calorimetry using scintillating plastic fibres," pp. 530–533, 1984.
- 411 [15] C. J. Werner *et al.*, "MCNP Version 6.2 Release Notes," Los Alamos, NM (United States), Feb. 2018.
- 412 [16] X. Mougeot, "Reliability of usual assumptions in the calculation of β and ν spectra," *Phys. Rev. C*, vol. 91,
413 no. 5, p. 055504, May 2015.
- 414 [17] M. J. Berger, J. . Coursey, M. . Zucker, and J. Chang, "ESTAR, PSTAR, and ASTAR: Computer Programs
415 for Calculating Stopping-Power and Range Tables for Electrons, Protons, and Helium Ions (version 1.2.3)," *National Institute of Standards and Technology, Gaithersburg, MD*. [Online]. Available:
416 <http://physics.nist.gov/Star>. [Accessed: 04-Jul-2021].
- 417 [18] M. R. Gupta, "Theory and Use of the EM Algorithm," *Found. Trends® Signal Process.*, vol. 4, no. 3, pp.
418 223–296, 2011.
- 419 [19] M. Frandes, B. Timar, and D. Lungeanu, "Image Reconstruction Techniques for Compton Scattering Based
420 Imaging: An Overview [Compton Based Image Reconstruction Approaches]," *Curr. Med. Imaging Rev.*,
421 vol. 12, no. 2, pp. 95–105, 2016.
- 422 [20] L. K and C. R, "EM reconstruction algorithms for emission and transmission tomography," *J. Comput.
423 Assist. Tomogr.*, vol. 8, no. 2, pp. 306–316, 1984.
- 424 [21] L. Bouchet, "A comparative study of deconvolution methods for gamma-ray spectra," *Astron. Astrophys.
425 Suppl. Ser.*, vol. 113, pp. 167–183, 1995.
- 426 [22] L. J. Meng and D. Ramsden, "An inter-comparison of three spectral-deconvolution algorithms for gamma-
427 ray spectroscopy," in *IEEE Nuclear Science Symposium. Conference Record. 1999 Nuclear Science
428 Symposium and Medical Imaging Conference (Cat. No.99CH37019)*, 1999, vol. 2, pp. 691–695.
- 429 [23] H. Lemaire, "Développement d'une caméra gamma de troisième génération," p. 206, 2015.
- 430 [24] Saint-Gobain, "Scintillating Optical Fibres," *Product Datasheet*. [Online]. Available:
431 <https://www.crystals.saint-gobain.com/sites/imdf.crystals.com/files/documents/fibre-product-sheet.pdf> .
- 432 [25] ET Enterprises, "9205B series data sheet," *Product Datasheet*. [Online]. Available: [http://et-
433 enterprises.com/images/data_sheets/9205B.pdf](http://et-enterprises.com/images/data_sheets/9205B.pdf) .
- 434 [26] CAEN, "DT5743," *Product Datasheet*. [Online]. Available: <https://www.caen.it/products/dt5743/>.

436 [27] M.-M. Bé and V. Chisté, "Table de radionucléides," *LNE-LNHB/CEA*, 2007.
437